Cardiomyocyte intracellular cholesteryl ester accumulation promotes tropoelastin physical alteration and degradation: Role of LRP1 and cathepsin S.

Valérie Samouillan, Elena Revuelta-López, Jany Dandurand, Laura Nasarre, Lina Badimon, Colette Lacabanne, Vicenta Llorente-Cortés

http://dx.doi.org/10.1016/j.biocel.2014.09.005

Cardiomyocyte intracellular cholesteryl ester accumulation promotes tropoelastin physical alteration and degradation Role of LRP1 and cathepsin S

Valerie Samouillan[a,*], Elena Revuelta-López[b,1], Jany Dandurand[a], Laura Nasarre[b], Lina Badimon[b], Colette Lacabanne[a], Vicenta Llorente-Cortés[b]

[a] *Physique des Polymères, Institut Carnot, CIRIMAT UMR 5085, Université Paul Sabatier, Bat 3R1B2, 118 route de Narbonne, 31062 Toulouse Cedex 04, France*
[b] *Cardiovascular Research Center, CSIC-ICCC, IIB-Sant Pau, Hospital de la Santa Creu i Sant Pau, 08025 Barcelona, Spain*

Keywords:
VLDL
Tropoelastin
Cathepsin S
Intracellular cholesterol esters
Cardiomyocyte
Cardiac remodeling

A B S T R A C T

Dyslipemia has a direct impact on cardiac remodeling by altering extracellular matrix (ECM) components. One of the main ECM components is elastin, a proteic three-dimensional network that can be efficiently degraded by cysteine proteases or cathepsins. Dyslipemic status in insulin resistance and combined hyperlipoproteinemia diseases include raised levels of very low density lipoproteins (VLDL), triglyceride (TG)-cholesteryl ester (CE)-rich lipoproteins. Enhanced VLDL concentration promotes cardiomyocyte intracellular cholesteryl ester (CE) accumulation in a LRP1-dependent manner. The aim of this work was to analyze the effect of cardiomyocyte intracellular CE accumulation on tropoelastin (TE) characteristics and to investigate the role of LRP1 and cathepsin S (CatS) on these effects. Molecular studies showed that LRP1 deficiency impaired CE selective uptake and accumulation from TG-CE-rich lipoproteins (VLDL + IDL) and CE-rich lipoproteins (aggregated LDL, agLDL). Biochemical and confocal microscopic studies showed that LRP1-mediated intracellular CE accumulation increased CatS mature protein levels and induced an altered intracellular TE globule structure. Biophysical studies evidenced that LRP1-mediated intracellular CE accumulation caused a significant drop of Tg2 glass transition temperature of cardiomyocyte secreted TE. Moreover, CatS deficiency prevented the alterations in TE intracellular globule structure and on TE glass transition temperature. These results demonstrate that LRP1-mediated cardiomyocyte intracellular CE accumulation alters the structural and physical characteristics of secreted TE through an increase in CatS mature protein levels. Therefore, the modulation of LRP1-mediated intracellular CE accumulation in cardiomyocytes could impact pathological ventricular remodeling associated with insulin-resistance and combined hyperlipoproteinemia, pathologies characterized by enhanced concentrations of TG-CE-rich lipoproteins.

1. Introduction

Extracellular matrix components such as fibrillar collagen, elastin, and proteoglycans play a wide variety of functions in the cardiovascular system, not only in the mechanics of the blood vessels but also in the heart (Fomovsky et al., 2010). One of the main extracellular matrix (ECM) proteins is elastin, a proteic three-dimensional network that has a relatively long turnover and half-life. In a situation of dyslipemia, vascular elastin suffers proteolytic degradation through the action of several proteases (Augier et al., 1997; O'Rourke, 2007; Fulop et al., 2012). Our group previously reported that, by inducing intracellular cholesteryl ester (CE) accumulation in human vascular cells, dyslipemic concentrations of LDL provoke crucial alterations in the molecular mobility of the soluble precursor of elastin, tropoelastin (TE) (Samouillan et al., 2012). Intracellular CE accumulation depends on the expression of low-density lipoprotein receptor-related protein (LRP1), a receptor that is essential for the uptake of aggregated LDL-CE by human vascular

* Corresponding author. Tel.: +33 561556816; fax: +33 561556221.
E-mail addresses: valerie.samouillan@univ-tlse3.fr (V. Samouillan), cllorente@csic-iccc.org (V. Llorente-Cortés).
[1] These authors have contributed equally to the manuscript.

smooth muscle cells (hVSMC) (Llorente-Cortés et al., 2002, 2006) and of very low density lipoprotein (VLDL) by HL-1 cardiomyocytes (Cal et al., 2012).

High plasma VLDL level is a prevalent characteristic in insulin-resistance (Goldberg, 2001) and combined hyperlipoproteinemia states (Jarauta et al., 2012). Perfusion of hearts with TG-enriched lipopoproteins reproduces the metabolic abnormalities of myocardial steatosis (Pillutla et al., 2005). Myocardial steatosis (Granér et al., 2013) and ECM remodelling (Hayden et al., 2006) are crucial events in the cardiometabolic syndrome. Myocardial steatosis, in particular, is considered an independent predictor of diastolic dysfunction in diabetic patients (Rijzewijk et al., 2008). Few studies have analyzed whether or how lipids alter ECM components such as TE, in the myocardium. TE is a key determinant of the response of the heart to mechanical stimulus (Gupta and Grande-Allen, 2006). TE contains one-third glycine amino acids (Sandberg, 1976) and several lysine derivatives that serve as covalent cross-link between protein monomers (Foster et al., 1974). Elastin is considered a three-dimensional network with 60–70 amino acids between two cross-linking points, with the alternation of hydrophilic cross-linking domains and dynamic hydrophobic domains with fluctuating turns, buried hydrophobic residues and main-chain polar atoms forming hydrogen bonds with water (Debelle and Tamburro, 1999; Li and Daggett, 2002; Floquet et al., 2004; Tamburro et al., 2006). This peculiar molecular architecture determines its elastic properties, insolubility and resistance to proteolysis (Mecham, 1991). It is known that pathological conditions such as acute ischemia (Sato et al., 1983) and pressure overload (Henderson et al., 2007) promote elastic fiber disruption. Elastin fragmentation causes plaque rupture and myocardial infarction in a mice model of atherosclerosis (Van der Donckt et al. 2014). Cathepsins (B, S, L and K) are cystein proteases with a high capacity to degrade extracellular matrix proteins such as elastin and fibrillar collagens (Obermajer et al., 2008). An imbalance of cathepsins and cystatins underlies myocardial remodelling associated with dilated (Ge et al., 2006), ischemic (Sun et al., 2011) and hypertensive cardiomyopathy (Cheng et al., 2006; Díez, 2010). We have previously shown that Cathepsin S (CatS) is strongly increased in lipid-loaded hVSMC and that these high CatS levels may contribute to the strong capacity of lipid-loaded hVSMC to cause elastin fragmentation (Samouillan et al., 2012). Despite the potential role of intracellular lipids on cardiac elastin and cardiac remodelling, the effect of cardiomyocyte intracellular lipids on tropoelastin characteristics is unknown. The aim of this work was to analyze the effect of cardiomyocyte intracellular CE accumulation on the physical characteristics of tropoelastin (TE) and to investigate the role of LRP1 and CatS on these effects.

2. Materials and methods

2.1. Cellular and molecular biology techniques

2.1.1. HL-1 cardiomyocyte cell culture

The murine HL-1 cell line was generated by Dr. W.C. Claycomb (Louisiana State University Medical Centre, New Orleans, Louisiana, USA) and kindly provided by Dr. U Rauch (Charité-Universitätmedizin Berlin). These cells show cardiac characteristics similar to those of adult cardiomyocytes (Claycomb et al., 1998). HL-1 cells were maintained in Claycomb Medium (JRH Biosciences, Lenexa, KS, USA) supplemented with 10% fetal bovine serum (FBS) (Invitrogen Corporation, Carlsbad, CA, USA), 100 μM norepinephrine, 100 units/mL penicillin, 100 μg/mL streptomycin, and L-glutamine 2 mM (Sigma Chemical Company, St. Louis, MO, USA) in plastic dishes, coated with 12.5 μg/mL fibronectin and 0.02% gelatin, in a 5% CO_2 atmosphere at 37 °C.

2.1.2. Zucker diabetic fatty rats

We purchased 7-week-old male ZDF (diabetic animals) and ZDFc (control) rats from Charles River Laboratories (L'Arbresle Cedex, France). Heart from these animals was obtained and immediately frozen at −80 °C. Different aliquotes of homogenized tissue were used to perform lipidic, molecular and physical analysis.

2.1.3. Generation of LRP1-deficient cardiomyocytes

2.1.3.1. Design of LRP1 miRNA lentiviral vectors. Three miR RNAi (XM_8531) sequences were designed to downregulate LRP1 (Accession number. XM_001056970) and cloned into pLenti6.4-CMV-MSGW (Invitrogen). We also used previously described (Cal et al., 2012) universal insert negative control (Invitrogen, pcDNA^{TM}6.2-GW/miR negative control).

2.1.3.2. Lentiviral particle production. Lentiviral particle production was performed as previously described with some modifications (Vilalta et al., 2009).

2.1.3.3. LRP1-deficient cardiomyocytes generation. Lentivirus stocks and a negative control generated from the resulting constructs were tittered by blasticidin selection. To generate a stock of LRP1-deficient HL-1 cells, they were stably transduced with 10 MOI lentivirus and maintained in a complete medium supplemented with blasticidin (10 μg/mL) to select blasticidin-resistant colonies. HL-1 cell clones with maximal LRP1 downregulation were selected, grown with blasticidin and used in further experiments. Control and LRP1-deficient HL-1 cardiomyocytes (i8531) were exposed to VLDL + IDL or agLDL (1.8 mM cholesterol, 18 h) and harvested by scraping in TriPure Reagent (Roche) for PCR and Western blot analysis.

2.1.4. Small interference RNA-mediated gene silencing of CatS in HL-1 cardiomyocytes

To inhibit CatS expression in HL-1 cardiomyocytes, cells were transiently transfected with annealed siRNA (siRNA-CatS) (AM16708) synthesized by Life Technologies. A siRNA-random was used as a negative control (Ambion AM 4636) in cellular transfections. Quiescent HL-1 cells were transfected with siRNA by the nucleofection technique using the Cell Line Nucleofector Kit L from Amaxa (VCA-1005) according to the manufacturer's instructions. The final siRNA transfection concentration for siRNA-CatS was 0.6 μmol/L. After 48 h of transfection, cells were exposed to lipoproteins and harvested by scraping in TriPure Reagent (Roche) for PCR and Western blot analysis.

2.1.5. Lipoprotein isolation and characterization

Lipoproteins were obtained from pooled sera of healthy normolipemic donors who gave their written informed consent. Only samples with a total cholesterol <5.2 mmol/L and triglycerides <1 mmol/L were pooled and frozen. Chylomicrons were firstly separated by ultracentrifugation of human plasma at 100.000 × *g* for 30 min at 4 °C. TG-CE-rich lipoproteins (VLDL + IDL) ($d_{1.001}$–$d_{1.019}$ g/mL) and LDL ($d_{1.019}$–$d_{1.063}$ g/mL) were obtained by sequential flotation ultracentrifugation for 20 h at 36,000 rpm at 4 °C.

Lipoproteins used in the experiments were less than 24 h old and have no detectable levels of endotoxin (Limulus Amebocyte Lysate test, Bio Whittaker). AgLDL was prepared by vortexing LDL in PBS at room temperature. The formation of LDL aggregates by vortexing was monitored by measuring the turbidimetry (absorbance at 680 nm) as previously described (Llorente-Cortés et al., 2002, 2004). Characterization of TG-CE rich lipoproteins and agLDL including lipids (cholesterol, triglycerides and phospholipids) and apolipoprotein B-100 (apoB) content was

performed by commercial standardized methods (Roche Diagnostics, Switzerland; Wako Chemicals, Germany) adapted to a Cobas c501 autoanalyzer.

2.1.6. Lipid extraction and determination of cholesterol esters (CE), triglycerides (TG) and free cholesterol (FC) content of cardiomyocytes

Quiescent HL-1 cells (4×10^4 cells/cm^2) were exposed to TG-CE-rich lipoproteins (1.8 mM cholesterol) and agLDL (1.8 mM cholesterol). HL-1 cardiomyocytes were exhaustively washed and harvested in NaOH 0.1 M. Lipids from rat myocardium and HL-1 cardiomyocytes were extracted as previously described (Cal et al., 2012) and CE, FC and TG content was analyzed by thin layer chromatography. The organic solvent was removed under N_2 stream, the lipid extract was redissolved in dichloromethomethane and one aliquot was partitioned by thin layer chromatography (TLC). TLC was performed on silica G-24 plates. The different concentrations of standards (a mixture of cholesterol, cholesterol palmitate and triglycerides) were applied to each plate. The chromatographic developing solution was heptane/diethylether/acetic acid (74:21:4, v/v/v). The spots corresponding to cholesteryl esters (CE), triglycerides (TG) and free cholesterol (FC) were quantified by densitometry against the standard curve of cholesterol palmitate, triglycerides and cholesterol, respectively, using a computing densitometer.

2.1.7. Western blot analysis

Blots were incubated with monoclonal antibodies against LRP1 β-chain (Fitzgerald; 10R-L107c, clone 8B8) or CatS (SANTA CRUZ BIOTECHNOLOGY Inc. Santa Cruz, CA; sc-271619; dilution 1:100). CatS (E-3) is a mouse monoclonal antibody specific for an epitope mapping between aminoacids 302-331 at the C-terminus of CatS and recognizes precursor (37 kDa) and mature (24 kDa) forms of CatS. To test equal protein loading for the different samples, blots were also incubated with monoclonal antibodies against β-tubulin (Abcam Ab6046).

2.1.8. Indirect immunofluorescence

Indirect immunofluorescence experiments were performed on cells grown in β-dish culture plates (Cal et al., 2012, Martinsried, Germany). Quiescent HL-1 cells were prechilled to 4 °C and washed with cold Claycomb medium containing 1% BSA (M199-BSA). HL-1 cells were incubated with 50 μg/mL DiI-(VLDL + IDL) at 4 °C for 30 min. After binding, medium was removed, and cells were incubated at 37 °C for 8 h in the absence or presence of DiI-(VLDL + IDL). Cells were then washed in Claycomb-BSA containing 100 U heparin/mL for 15 min at 4 °C with constant shaking. They were then fixed at room temperature for 10 min in PBS containing 3% paraformaldehyde and 2% sucrose before staining with Hoechst 33258 colorant (1:2000) for 10 min, and washed twice with PBS. After DiI-(VLDL + IDL) incubation, several samples were stained with anti-LRP β-chain antibodies (Abcam, Ab92544) to analyze the colocalization of DiI-(VLDL + IDL) and LRP1. In a set of experiments, fixed cells were permeabilized and incubated with antibodies against tropoelastin (Santa Cruz Biotechnology, Inc.; sc-17580) and CatS (Santa Cruz Biotechnology, Inc.; sc-271619) for 1 h. Cultures were then incubated for an additional hour with secondary polyclonal antibodies; anti-goat polyclonal (Molecular Probes, rabbit anti-goat 633) and anti-mouse monoclonal (donkey anti-mouse 488) antibodies.

Samples were analyzed by a laser-scanning confocal fluorescence microscope (Leica TCS NT). The software program used was TCSNT, version 1.3.237 (Leica).

2.2. Physical techniques

HL-1 cell supernatants were centrifuged at 3000 × g for 5 min at RT to remove lipids not taken up by the cells. The pellet was discarded and the remaining supernatant was freeze–dried and used for supernatant TE physical characterization. Homogenized freeze–dried rat myocardium was used for FTIR/ATR analysis. Results from DSC analysis were not reported because of the low signal of intrinsic transitions due to a weak mass of sample.

2.2.1. Fourier transform infrared analysis (FTIR)

Fourier transform infrared spectroscopy/attenuated total reflectance (FTIR/ATR) spectra were acquired using a Nicolet 5700 FTIR (THERMO FISHER SCIENTIFIC, Waltham, MA) equipped in ATR device with a KBr beam splitter and a MCT/B detector. The ATR accessory used was a Smart Orbit with a type IIA diamond crystal (refractive index 2.4). Spectra were recorded over the region of 4000–450 cm^{-1} with a spectral resolution of 4 cm^{-1} and 80 accumulations. Spectral data were collected using Omnic 7.3 (THERMO FISHER SCIENTIFIC, Waltham, MA). A single-beam background spectrum was collected from the clean diamond crystal before each experiment and this background was subtracted from the spectra. Spectra were then subjected to ATR and baseline corrections and normalized in the amide I region. For each type of supernatant or tissue, a mean representative spectrum and its second derivative were computed. Second derivatives were used to enhance the chemical information present in overlapping infrared absorption bands of spectra and to circumvent baseline drifts in infrared spectra. Absorption bands were identified using data on biological tissues, protein and peptides FTIR absorption bands (Yu and Kalnin, 1990; Barth, 2000, 2007; Servaty et al., 2001; Hu et al., 2006; Bonnier et al., 2008; Popescu et al., 2010; Sionkowska et al., 2010; Staniszewska et al., 2014). Supplemental Table S1 lists the position and probable assignments for the bands of the supernatants of control cardiomyocytes.

2.2.2. Thermogravimetric analysis (TGA)

Analyses were performed in alumina pans, with an initial mass of 7 mg, between 25 and 650 °C at 10 °C/min under N_2 atmosphere using a TGA Q50 (TA INSTRUMENTS, New Castle, DE).

2.2.3. Differential scanning calorimetry (DSC)

Analyses were performed using a DSC Pyris calorimeter (PERKIN ELMER, Waltham, MA) The calorimeter was calibrated using Hg and In as standards, resulting in a temperature accuracy of ±0.1 °C and an enthalpy accuracy of ± 0.2 J/g. Samples, 5 mg in weight, were set into aluminium pans and equilibrated at the initial temperature for 5 min before heating at 20 °C/min. Transition parameters were processed using DSC Pyris calorimeter software.

2.3. Statistical analysis

Quantitative values are shown as means ± SEM. All experiments were performed with at least three replicates for each group and for at least three independent repeats. Student's *t*-test was used for statistical analysis and a *P*-value of less than 0.05 was considered statistically significant.

3. Results

3.1. Biochemical, molecular and cellular results

3.1.1. Biochemical characteristics of TG-CE rich lipoproteins (VLDL + IDL) and agLDL

TG-CE rich lipoproteins (VLDL + IDL) and agLDL differ mainly in CE, TG, PL and apoB content (Table 1). The relation cholesterol:TG

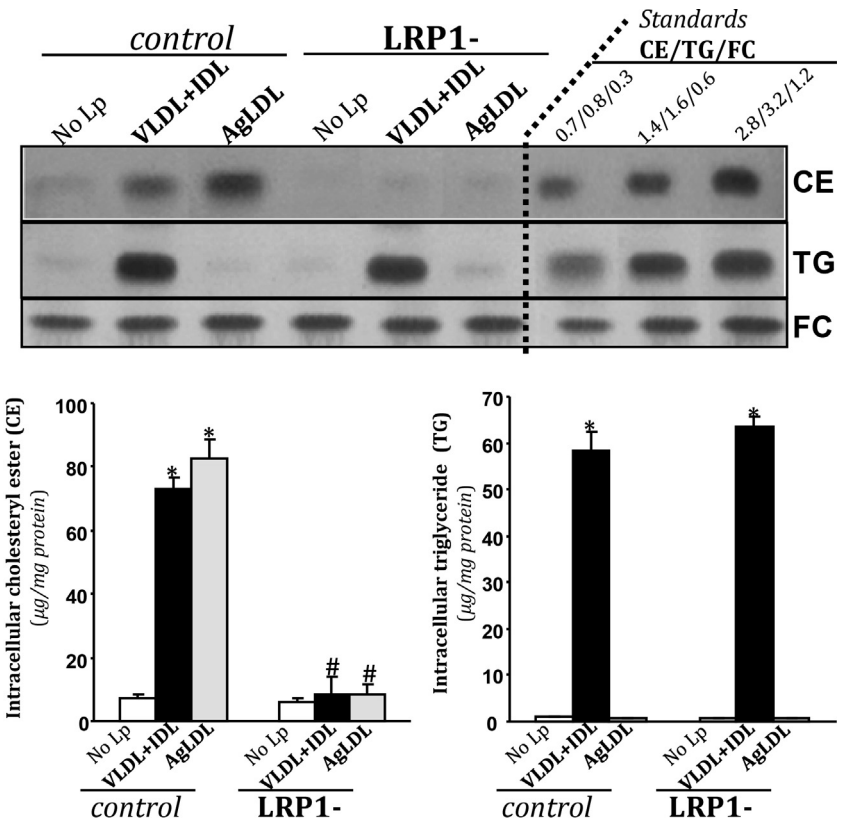

Fig. 1. Effect of VLDL + IDL and AgLDL on intracellular neutral lipid content of control and LRP1 deficient (LRP1−) HL-1 cells. Thin layer chromatography showing cholesteryl ester (CE), triglyceride (TG) and free cholesterol (FC) bands and histograms with their quantification. Results are expressed as micrograms per milligram of protein and shown as mean ± SEM of three experiments performed in triplicate. $^{*}P < 0.05$ *vs.* cells unexposed to lipoproteins. $^{\#}P < 0.05$ *vs.* control cells.

Table 1
Relative lipid composition of VLDL + IDL and agLDL.

	Chol	PL	TG	ApoB
VLDL + IDL	3.54 ± 0.03	1.56 ± 0.17	3.33 ± 0.04	0.45 ± 0.00
AgLDL	7.76 ± 1.49	1.93 ± 0.12	1.06 ± 0.18	0.82 g/L

Cholesterol (Chol), phospholipid (PL) and triglyceride (TG) content of lipoproteins was measured in a Cobas c501 autoanalyzer. Results are the mean ± SD of three different samples. Chol, PL and TG are expressed as mM and ApoB as g/L.

is 1:1 for TG-CE rich lipoproteins (VLDL + IDL) and 7:1 for agLDL. As shown in Fig. 1, VLDL + IDL and agLDL caused a differential pattern of intracellular neutral lipid accumulation in HL-1 cardiomyocytes. VLDL + IDL induced a strong intracellular CE and TG accumulation while agLDL exclusively induced intracellular CE accumulation in HL-1 cardiomyocytes. LRP1 deficiency prevented VLDL + IDL- and agLDL-induced intracellular CE accumulation. However, LRP1 deficiency did not exert any significant effect on VLDL + IDL-induced intracellular TG accumulation.

3.1.2. LRP1-mediated cardiomyocyte intracellular CE accumulation increases CatS mature protein levels and alters the structure of TE secretory globules

Western blot analysis showed that VLDL + IDL (1.8 mM Chol) and agLDL (1.8 mM Chol) increased mature CatS protein levels in an LRP1-dependent manner in HL-1 cardiomyocytes (Fig. 2). It has been previously reported that TE aggregates have a characteristic peri-nuclear appearance of secretory pathway components, and that the organization of these aggregates in globules is a required step for elastin organization (Davis and Mecham, 1998; Kozel et al., 2006). Confocal microscopy experiments (Fig. 3) showed that TE was secreted in this globular pattern (asterisks) by HL-1 cardiomyocytes unexposed to lipoproteins (panel a). In contrast, TE globule structure was altered in VLDL + IDL- (panel b) and in agLDL (panel c)-loaded cardiomyocytes. LRP1 deficiency prevented these alterations and rescued the original TE globule structure in cardiomyocytes exposed to VLDL + IDL (panel e) and agLDL (panel f).

3.1.3. CatS mediates the deleterious effect of cardiomyocyte intracellular CE accumulation on TE globule structure

As shown in Fig. 4, CatS silencing prevented the alterations of TE globule structure induced by VLDL + IDL- (panel b) and agLDL (panel c)-loading of cardiomyocytes and rescued the original TE globule structure in VLDL (panel e) and agLDL (panel f)-loaded cells. These results indicate that cardiomyocyte intracellular CE accumulation induces structural alterations in TE through the upregulation of CatS mature protein levels.

3.2. Physical results

3.2.1. Physical characteristics of HL-1 cardiomyocyte supernatants

The classical absorption bands of proteins (amide A, amide I, II, III) were found on the spectra of control, LRP1- and CatS-cardiomyocytes, and their positions were very close to the absorption bands of the supernatant from hVSMC (superimposed on Fig. S1A and S1B) mainly constituted of tropoelastin (Samouillan et al., 2012). The main difference with pure tropoelastin concerned the broad band located at 1591 cm^{-1} on the global spectra of all supernatants (Fig. S1B). Position and probable bands assignments of the supernatants from control cardiomyocytes are listed in Table S1.

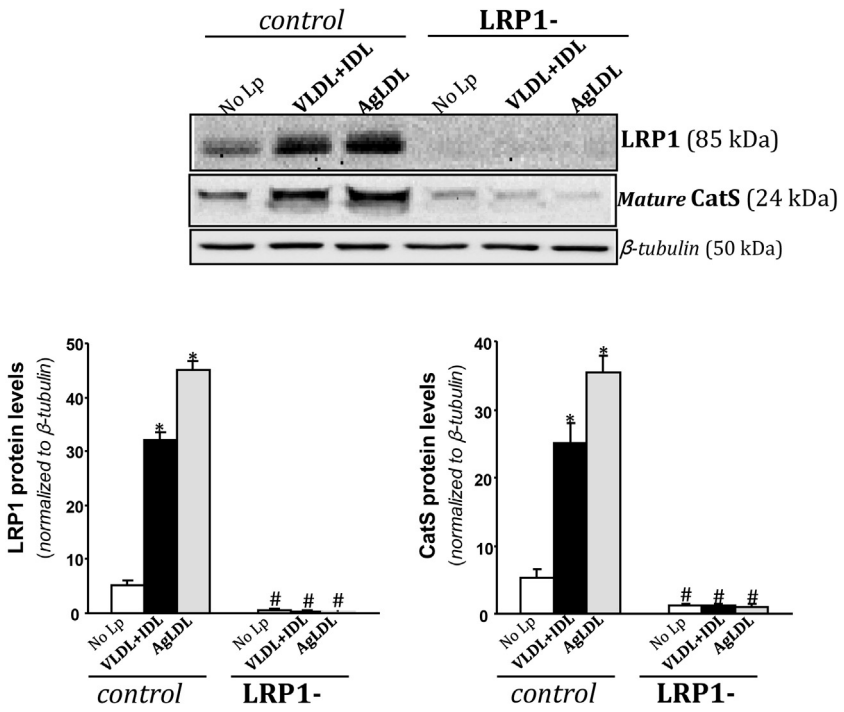

Fig. 2. Effect of VLDL + IDL and AgLDL on LRP1 and CatS protein levels of control and LRP1 deficient (LRP1−) HL-1 cells. Representative Western blot analysis showing LRP1 and mature CatS protein levels in control and LRP1-cells. Bar graphs showing the quantification of LRP1 and CatS normalized by β-tubulin bands. Results are expressed as arbitrary units and shown as mean ± SEM of three experiments performed in triplicate. $^{*}P < 0.05$ *vs.* cells unexposed to lipoproteins. $^{\#}P < 0.05$ *vs.* control cells.

The comparison of the second derivative spectra in the amide I/amide II (Fig. 5A), which are sensitive to secondary structures, confirmed the close correlation between the chemical composition of cardiomyocyte and hVSMC supernatants. Spectral supernatant signature was similar in HL-1 cardiomyocytes, hVSMC and elastic tissues that have the main minima of the amide I at 1694 cm^{-1} (anti-parallel β sheets), 1684 cm^{-1} (anti-parallel β sheets and β turns), 1669 cm^{-1} (undefined or β turns), 1652 cm^{-1}

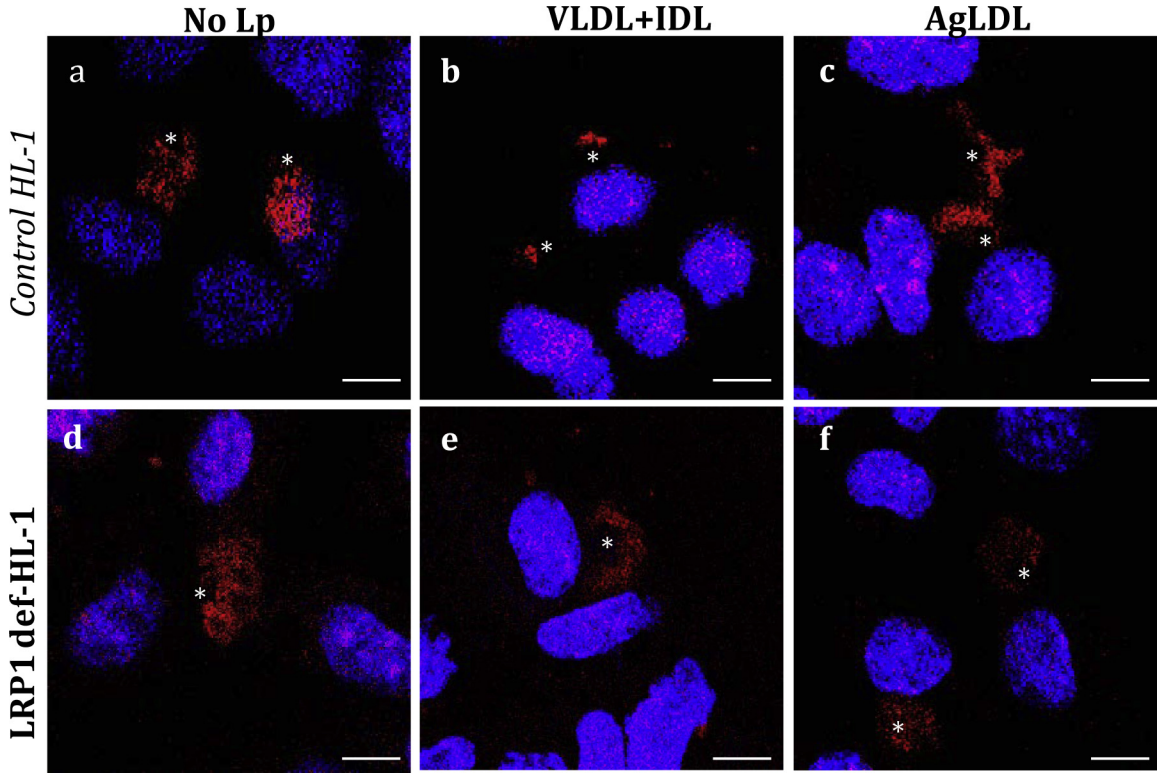

Fig. 3. Effect of VLDL + IDL and AgLDL on tropoelastin (TE) in control and LRP1 deficient (LRP1−) HL-1 cells. Representative confocal microscopy images showing the globular structure of TE (in red) synthesized and secreted by HL-1 cardiomyocytes. Asterisks show TE structures. Nuclei are in blue. Bar scale: 10 μm (For interpretation of the color information in this figure legend, the reader is referred to the web version of the article.).

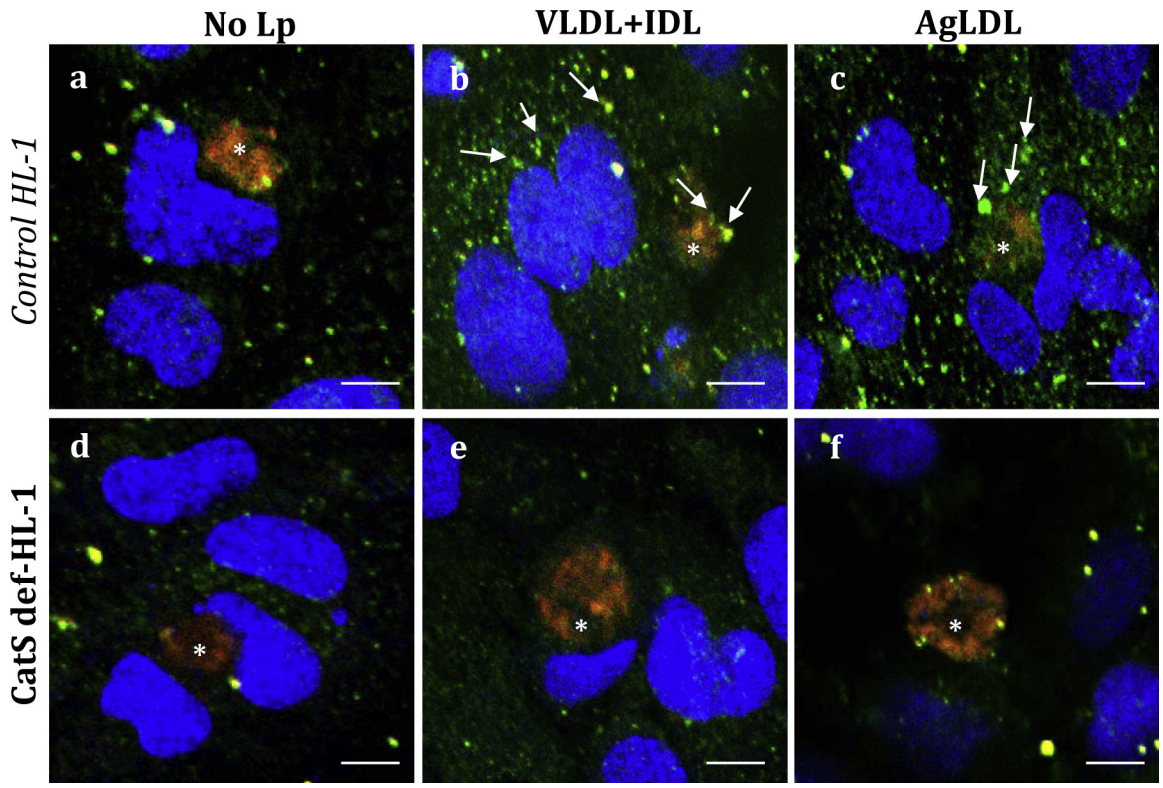

Fig. 4. Effect of VLDL + IDL and AgLDL on tropoelastin (TE) in control and CatS deficient (CatS−) HL-1 cells. Representative confocal microscopy images showing CatS (in green) and TE (in red) in HL-1 cardiomyocytes. Asterisks show TE structures and arrows CatS staining. Nuclei are in blue. Bar scale: 10 μm (For interpretation of the color information in this figure legend, the reader is referred to the web version of the article.).

(α helices), 1636 cm^{-1} (hydrated water/intramolecular β sheets) and 1617 cm^{-1} (β turns) and the main minima of the amide II at 1559 (β sheets), 1542 cm^{-1} (unordered or α helices) and 1516 cm^{-1} (anti parallel β sheets) (Debelle et al., 1995; Herberhold and Winter, 2002; Bonnier et al., 2006; Pluot et al., 2007; Staniszewska et al., 2014). The presence of these secondary structures was confirmed by the Amide III analysis (not shown) presenting main minima at 1317 cm^{-1} (α helices), 1258 cm^{-1}, 1221 cm^{-1} (β sheets) and 1280 cm^{-1} (random). The main difference with pure tropoelastin concerned the associated minima on the second derivative in the same wavenumber range (Fig. 5A), which can be attributed to glycoaminoglycans, free amino acids and/or proteins rich in His, Phe, His and Gln. The second derivative spectra of control cardiomyocytes in the 3000–2800 cm^{-1} (Fig. 5B) corresponded to the region of asymmetric and symmetric vibrations of methyl and methylene groups (mainly from Gly, Pro, Val, Ala, Leu) of proteins. In control supernatants, the more visible minimum at 2931 $cm-^{1}$ corresponded to asymmetric CH_2 stretching.

Thermogravimetric (TG) and temperature/derivative (DTG) plots of purified supernatants from control and VLDL-loaded mice cardiomyocytes are shown in Fig. S2. Since this technique is very mass-consuming, we first performed it only in control cardiomyocytes to set the limits of DSC analyses (below the degradation temperature) and to detect eventual evolution of the degradation process with lipid-loading. The global trend of the two TG plots corresponded to the classical thermal behavior of freeze–dried proteins (Puett et al., 1967; Samouillan et al., 1999). The first stage (between 25 and 100 °C) is connected with the evaporation of water absorbed to the protein, while the second stage is associated with a multi-step stage corresponding to the degradation of the sample, namely a deamination and a depolymerization arising from the breaking of polypeptide bonds. It is noteworthy that these two fractions begin to degrade at 100 °C (with the presence of well-marked peaks on the derivative DTG curves in the 100–220 °C zone), in contrast with the supernatant from hVSMC mainly constituted of tropoelastin (superimposed in Fig. S2) that remains stable up to 250 °C, as usually observed in elastin fractions (Samouillan et al., 1999, 2012). This multiple degradation processes in the 100–220 °C was indicative of the presence of less stable components than tropoelastin in cardiomyocyte supernatants, corroborating FTIR results. In our previous study on the thermal degradation of hVSMC supernatants, the two degradations peaks at 313 and 335 °C were attributed to non-aggregated and aggregated tropoelastin, respectively. In the present study, only subsist in this temperature zone the degradation peak associated with non-aggregated tropoelastin, occurring between 311 and 313 °C for the two fractions.

As shown in Fig. 6, two major glass transitions were observed in control HL-1 cardiomyocyte supernatants as a step of the heat flow. The glass transition mean temperatures Tg determined from a statistical analysis are reported in Fig. 7. The presence of two glass transitions was indicative of two kinds of amorphous phases in the purified supernatants. According to literature data on the calorimetric and mechanical properties of proteins of the extracellular matrix and tissues (Hoeve and Flory, 1974; Samouillan et al., 1999; Lillie and Gosline, 2002a, 2002b; Hu et al., 2010; Panagopoulou a et al., 2013), the presence of a glass transition in the 30–200 °C range (related to the hydration state and micro-environment) is generally associated with the signature of elastin or gelatin (denatured collagen). This thermal event, addressed to the amorphous, unordered zones of polymers and biopolymers, characterizes the zone of viscoelasticity of materials. Elastin does not possess a long range order, and although different secondary conformations can be found in this protein, it can be considered as amorphous for the physical structure, which is in good agreement with the Tamburro's model on labile, dynamic β turns in hydrophobic domains (Debelle and Tamburro, 1999; Tamburro et al., 2006) and the Daggett's model

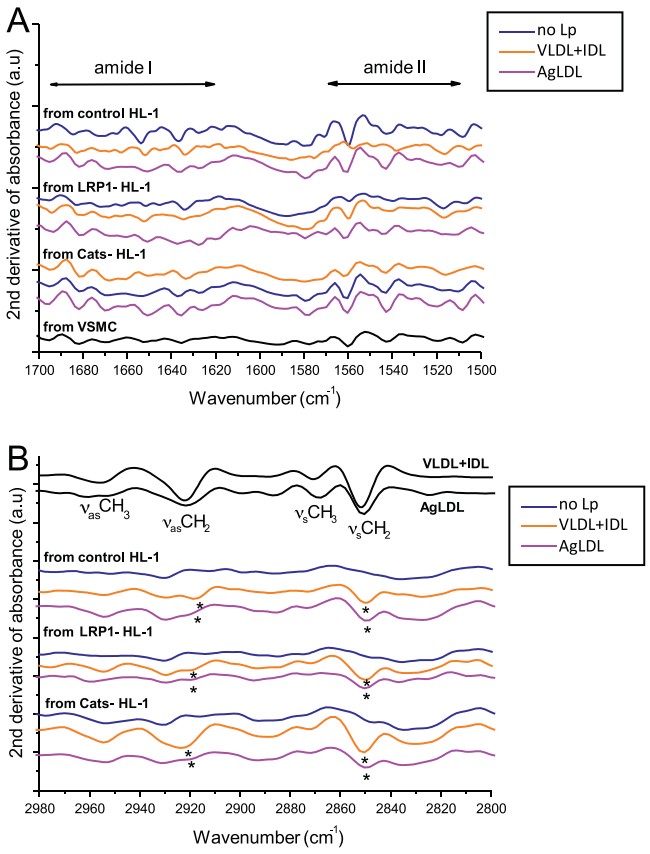

Fig. 5. Effect of VLDL + IDL and AgLDL on the second derivative FITR spectra of control and LRP1 deficient (LRP1−) HL-1 cells. Second derivative FTIR spectra in the 1700–1500 cm^{-1} zone (A) and in the 3000–2800 cm^{-1} zone (B). Thin lines: VLDL + IDL, AgLDL and supernatants from VSMC; bold lines: supernatants from the different sets of HL-1 cardiomyocytes. Asterisks label the vibrations that are specific of methylene groups present in lipoproteins.

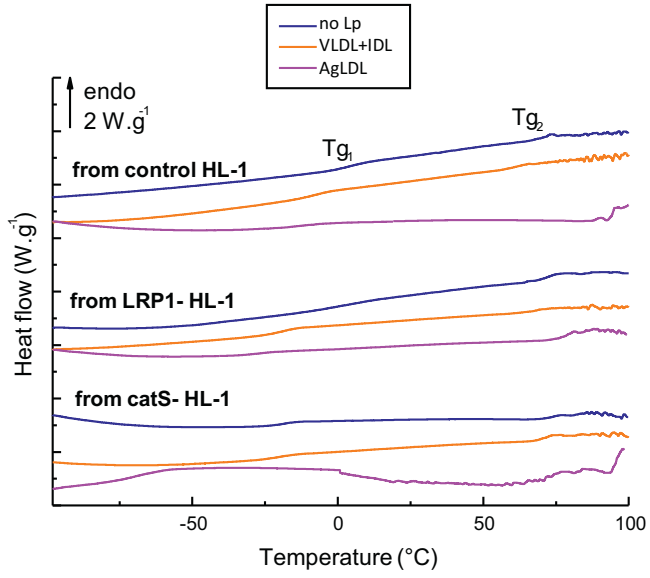

Fig. 6. Effect of VLDL + IDL and AgLDL on DSC thermograms of supernatants from control, LRP1 deficient (LRP1−) and CatS deficient (CatS−) HL-1 cells. Differential Scanning calorimetry thermograms of VLDL + IDL, AgLDL and supernatants from the different sets of HL-1 cardiomyocytes. Pseudo-second-order transitions are marked as Tg1 and Tg2.

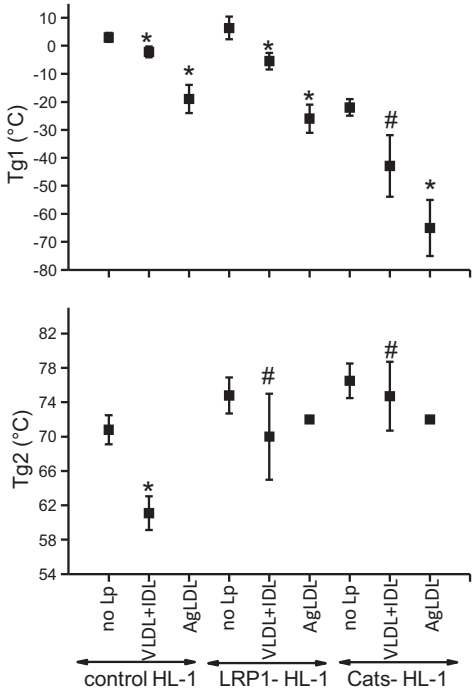

Fig. 7. Effect of VLDL + IDL and AgLDL on glass transition temperatures of supernatants from control, LRP1 deficient (LRP1−) and CatS deficient (CatS−) HL-1 cells. Glass transition temperatures (Tg1 and Tg2) from DSC analysis of the purified supernatants from the different sets of HL-1 cardiomyocytes. $^{*}P < 0.05$ *vs.* cells unexposed to lipoproteins. $^{\#}P < 0.05$ *vs.* control cells.

(Li, 2002) that describes hydrophobic domains of elastin as compact amorphous structures. According to previous work on supernatants from hVSMC (Samouillan et al., 2012), the higher glass transition Tg2 recorded at 68 °C for supernatants from control cardiomyocytes can be thus attributed to non-aggregated tropoelastin. The presence of a second, lower glass transition temperature Tg1 recorded at 4 °C for supernatants from control cardiomyocytes attests to a phase segregation in the supernatants, and although its origin is unclear it could be tentatively assigned to flexible macromolecules like glycosaminoglycans, or low molecular weight polypeptides.

3.2.2. Physical characteristics of TG-CE rich lipoproteins (VLDL + IDL) and agLDL

The pure VLDL + IDL and agLDL FTIR spectra superimposed on supplemental Figs. S1A and Fig. S1B fit well with literature data showing specific absorption of the carbonyl stretching of ester bond at 1743 and 1737 cm^{-1}, respectively. This spectra has been attributed to phospholipids, unsaturated triglycerides and cholesteryl esters (Nara et al., 2002; Krilov et al., 2009). The shift of 6 cm^{-1} between VLDL + IDL and agLDL has been ascribed to the difference in the surroundings and dynamics of carbonyl groups (Nara et al., 2002), due to the distinct chemical composition and packing of these lipoproteins. The thermogram of VLDL + IDL; was characterized by an exothermic first order transition at −70 °C, that can be ascribed to a crystallization phenomenon, followed by two endothermic first order transitions at 24.5 and −1 °C, respectively, corresponding to the order–disorder transitions of triglycerides exhibiting polymorphic behaviour as already noted in literature data (Hale and Schroeder, 1981; Prassl et al., 1995). The calorimetric signature of agLDL (**supplemental Fig. S3**) was completely distinct from the VLDL + IDL one, with a glass transition at Tg = −33 °C, ascribed to the amorphous phase of agLDL, and a single order-disorder transition at 38 °C. These data highlight the extreme difference between the physical structure of VLDL + IDL and agLDL.

3.2.3. Cardiomyocyte intracellular CE accumulation reduces TE Tg2 glass transition temperature in LRP1- and CatS-dependent manner

VLDL + IDL- and agLDL-loading of control cardiomyocytes decreases the TE Tg2 glass transition temperature in a significant manner ($p = 0.00375$) (Fig. 7). It must be pointed out that the glass transition Tg2 of supernatants from agLDL-loaded cardiomyocytes was not detected, indicating a dramatic effect of agLDL on TE physical structure. However, LRP1-deficiency prevented this downregulatory effect of VLDL and agLDL on TE Tg2 glass transition. Despite of the fact that variability is high, these results indicate that LRP1 plays a crucial role in the deleterious effect of VLDL and agLDL on TE Tg2 glass transition. It was not possible to achieve statistical analysis with results obtained in agLDL-loaded cardiomyocytes since the degradation process can induce erroneous values.

CatS silencing also prevented the downregulatory effect of VLDL and agLDL on TE Tg2 glass temperature (Figs. 6 and 7). These results indicate that cardiomyocyte intracellular CE accumulation induces physical alterations in TE through the upregulation of CatS mature protein levels.

3.2.4. Exogenous non-internalized VLDL + IDL and agLDL cause alterations in cardiomyocyte tropoelastin physical characteristics in an LRP1 and CatS-independent manner

As observed in the FTIR second derivative spectra of Fig. 5A, VLDL + IDL and agLDL did not induce differences in the main minima of supernatants, indicating that VLDL + IDL and agLDL did not alter cardiomyocyte TE secondary structure. Nevertheless, the complexity of the supernatant spectra makes difficult to use the decomposition of amide I as a method to identify modifications in the amount of α helices, β sheets-β turns and unordered structures induced by exogenous lipids. In the 1780–1700 cm^{-1} spectra enlarged zone (supplemental Fig. S1C) there was a shoulder located at 1740 cm^{-1} in supernatants from VLDL and agLDL-exposed cardiomyocytes. This shoulder remained in LRP1- ant CatS-deficient HL-1 cardiomyocytes, and reflected the presence of interacting lipids from VLDL and agLDL. The footprint of interacting exogenous lipids was also observed on the 3000–2800 cm^{-1} second derivative zone region (Fig. 5B) corresponding to vibrations of methyl and methylene groups. The specific signature of methylene groups in lipoproteins was detected at 2920 and 2850 cm^{-1} (asterisk). DSC measurements (Figs. 6 and 7) showed that the glass transition temperature, Tg1, ascribed to the softer phase – but not associated with native TE – was drastically decreased in HL-1 cardiomyocytes exposed to VLDL and even more so in those exposed to agLDL, in an LRP1 and CatS-independent manner.

3.3. In vivo results

We have tested the relevance of some of the *in vitro* findings in an *in vivo* model of diabetes. As shown in supplemental Fig. S4, there was a significant accumulation of neutral lipids (both CE and TG) in the myocardium of diabetic compared to control rats (Fig. S4A). Western blot analysis showed that both myocardial LRP1 and CatS mature protein levels were strongly higher in diabetic rats *versus* control rats (Fig. S4B). Finally, FITR analysis showing the comparison of the second derivative FTIR spectra in the amide I/amide II zone (sensitive to secondary structures) evidenced some significant and reproducible differences between heart tissue from control and diabetic rats (analyses performed in triplicate) (Fig. S5). The minima positions reported in supplemental Table S2 fit with collagen and elastin minima as well as with cardiovascular tissues. In heart tissues from diabetic rats, the vanishing of the bands at 1643and 1537 cm^{-1} can be associated with the lack of unordered structures. This could be associated with an alteration of elastin. Moreover, the slight shift of the bands at 1631 and 1547 cm^{-1} (β sheets) towards low wave number is ascribed to the enhancement of hydrogen bonding that could be due to an aggregation phenomenon. These results indicate that elastin in the heart of diabetic rats lost part of its characteristic random structure associated with entropic elasticity.

4. Discussion

This study shows that intracellular CE accumulation derived from TG-CE rich lipoproteins (VLDL + IDL) and agLDL raises CatS mature protein levels, alters the structure of intracellular tropoelastin globules and the physical characteristics of cardiomyocyte secreted tropoelastin. It also indicates that by impairing cardiomyocyte intracellular CE accumulation and CatS increase, LRP1 deficiency prevents physical alterations that make elastin prone to rupture. Our results suggest that cholesteryl ester-loaded cardiomyocytes induce physical alterations in myocardial tropoelastin that make elastin prone to rupture and that LRP1 is a crucial receptor in this process.

Our data consistently demonstrate that intracellular CE accumulation is one of the main intracellular neutral lipids modulating the physical characteristics of cardiomyocyte-secreted tropoelastin. First, we observed that VLDL + IDL- composed of CE and TG- and agLDL- composed of CE- exerted similar deleterious effects on CatS mature levels, TE structure and physical characteristics. Second, we found that these deleterious effects were LRP1 dependent. Previous studies from different groups including ours have demonstrated that LRP1 participates in the selective uptake of cholesteryl esters from lipoproteins (Swarnakar et al., 2001; Vassiliou and McPherson, 2004; Llorente-Cortés et al., 2006; Cal et al., 2012). LRP1-mediated CE selective uptake is a mechanism highly favoured by the capacity of LRP1 to interact with proteoglycans and lipases (Swarnakar et al., 2001; Nielsen et al., 1997), molecules that strongly facilitate CE selective uptake by promoting lipoprotein retention and modification (Sartipy et al., 1999; Kadowaki et al., 1992; Seo et al., 2000). Remarkably, CE and TG are taken up through different mechanisms in cardiomyocytes. While CE accumulation respond to VLDL-CE uptake through LRP1-mediated selective uptake (Cal et al., 2012), triglyceride accumulation responds to whole lipoprotein uptake through VLDLR and/or FA uptake though different FA transporters (Goldberg et al., 2011).

We emphasize that in the present study, we used TG-CE rich lipoproteins at enhanced concentrations. As these concentrations are characteristic of insulin resistance and combined hyperlipoproteinemia states, these lipoproteins may cause myocardial CE content and associated cardiac alterations in patients with these pathologies. Small lipoproteins enriched in CE and large lipoproteins enriched in TG potentially increase intracellular CE content. It is of note that not only the lipid composition but also lipoproteins size and protein composition may influence lipoprotein biological effects. It is also important to emphasize that fibroblasts, considered the main cellular type responsible for TE production in the heart (Eghbali, 1992), have a strong capacity to take up lipoproteins (Llorente-Cortés et al., 2002). This mechanism may thus be highly relevant for alterations in fibroblast secreted TE and cardiac remodeling. Our results also show that cardiomyocyte intracellular CE accumulation exerted deleterious effect of TE structure and physical characteristics through upregulation of CatS mature levels. CatS, like other cystein proteases, is expressed as inactive proenzyme that undergoes activation by the cleavage of the pro-domain under acidic conditions (Bromme, 2004). Exceptionally, CatS, remains catalytically active under neutral pH and remains stable outside the lysosome. Like CatB and CatL, CatS undergoes autoactivation (Pungercar et al., 2009). Interestingly, glycosaminoglycans promote the autocatalytic processing of

cathepsins to their mature forms (Caglic et al., 2007). Glycosaminoglycan structure depends on hyaluronan synthase (HAS), a unique membrane-associated glycosyltransferase whose activity is modulated by membrane cholesterol composition (Ontong et al., 2014). The culture of human dermal fibroblasts in lipoprotein-depleted medium seems to attenuate the synthesis of hyaluronan. Therefore, in our *in vitro* system, intracellular CE accumulation could increase HAS activity and hyaluronan content. High levels of glycosaminoglycans would induce the autocatalytic processing of CatS to their mature forms. This mechanism could explain why we exclusively detect the mature form of CatS in VLDL + IDL- and agLDL-loaded HL-1 cardiomyocytes. Further studies are required to know whether this mechanism plays a role in the activation of CatS by intracellular CE accumulation in HL-1 cardiomyocytes. The upregulatory effect of intracellular CE accumulation on CatS mature protein levels in cardiomyocytes has been previously shown in human VSMC (Samouillan et al., 2012) and macrophages (Burns-Kurtis et al., 2004). According to our results, CatS actively participates in the deleterious effect of VLDL + IDL and agLDL on tropoelastin globule structure. We show that VLDL + IDL and agLDL clearly altered the pattern of cardiomyocyte TE secretion and that CatS deficiency rescues the original TE globule structure. CatS effects on TE secretion are likely related to the capacity of this protease to control the trafficking and flow of certain proteins to the cell surface (Driessen et al., 1999). Our results support the theory about the possible active role of intracellular cathepsins in a process called "subcellular remodelling", already described in congestive heart failure (Dhalla et al., 2009).

DSC thermograms of supernatants showed that intracellular CE accumulation also influenced the physical characteristics of secreted TE. In particular, it caused a strong reduction of glass transition temperature Tg2, attributed to non-aggregated tropoelastin. According to the free volume theory, this plasticization phenomenon can be due to the insertion of compatible low molecular weight molecules or to the fragmentation of the main chain producing more end chains and thus increasing the free volume (Ferry, 1980). According to our physical data, this plasticization is due to the partial degradation of the tropoelastin chain. VLDL + IDL and agLDL did not cause this plasticization effect in LRP1- and CatS-deficient cardiomyocytes, which have normal TE globular structure. We thus propose that TE plasticization could be the result, at least in part, of CatS-induced structural alterations of intracellular TE globules. TE plasticization contributes to TE fragmentation and formation of elastin-derived peptides. Elastin-derived peptides reportedly increase atherosclerosis (Gayral et al., 2014) and modulate insulin-resistance (Blaise et al., 2013) in *in vivo* models. Additionally, CatS, a key player in this process, has been reportedly involved in ECM remodeling associated with dilated (Ge et al., 2006), ischemic (Sun et al., 2011) and hypertensive cardiomyopathy (Cheng et al., 2006; Díez, 2010). Our results from the *in vivo* model of diabetes showed that LRP1 and mature CatS protein levels were strongly increased in the myocardium of diabetic rats compared to controls. Moreover, we also found an strong myocardial cholesterol ester accumulation in the myocardium of diabetic rats. Additionally, FITR/AVR indicates that elastin in the heart of diabetic rats lost part of its characteristic random structure associated with entropic elasticity. Taken together, these results suggests that myocardial CE accumulation in the diabetic heart, by increasing CatS mature protein levels, may contribute to adverse myocardial remodelling in diabetes.

Besides these TE physical alterations induced by intracellular CE accumulation, we observed alterations both in lipoproteins and ECM that are independent on cellular CE uptake. These alterations are likely facilitated by a close interaction between lipoproteins and ECM. FTIR analysis indicates that a weak fraction of lipids remains after the purification of supernatants. The absence of the thermal transitions of pure VLDL + IDL or agLDL in the thermograms of the supernatants from VLDL + IDL- and agLDL-exposed cardiomyocytes suggests a modification of the physical structure of these lipoproteins, associated with their interaction with cellular or supernatant components, as previously reported for several lipoproteins and elastic materials (Podet et al., 1991; Lillie and Gosline, 2002a; Samouillan et al., 2012). This interaction between lipoproteins and cell/supernatant components could also explain the decrease of the Tg1 glass transition in VLDL and agLDL-exposed cardiomyocytes. Apart from the hydration effects, the presence of the lipid molecules inside the biological network would itself increase the network free volume, providing some direct plasticization (Lillie and Gosline, 2002a). A similar decrease in the glass transition temperature Tg1 associated with non-aggregated tropoelastin has been previously observed in supernatants of human VSMC exposed to modified lipoproteins (Samouillan et al., 2012). Tg1 decrease may be also associated to modifications of the physical structure of the elastic material, although, according to our results, this physical alteration is LRP1- and CatS-independent.

In summary, lipoprotein-derived neutral lipids influence physical characteristics of tropoelastin at both an intracellular and extracellular level. At the intracellular level, cholesteryl esters alter tropoelastin physical characteristics and promote tropoelastin fragmentation by increasing mature CatS protein levels.

Sources of funding

This work was funded by FIS PI11/00747 from Instituto Salud Carlos III, co-financed by the European Fund for Regional Development (E.F.R.D.) and by Red de Investigación Cardiovascular—RIC (RD RD12/0042/0027). V.L.L.-C. and L.B. are members of the Quality Research Groups from Generalitat de Catalunya 2014-SGR-170 and 2009-SGR-826, respectively.

Acknowledgements

The authors thank Dra. Esther peña (Cardiovascular Research Center, CSIC-ICCC) by her technical help with confocal microscopy experiments and Carolyn Newey (IIB Sant Pau) for editorial assistance.

Appendix A. Supplementary data

Supplementary data associated with this article can be found, in the online version, at http://dx.doi.org/10.1016/j.biocel.2014.09.005.

References

Augier T, Charpiot P, Chareyre C, Remusat M, Rolland PH, Garçon D. Medial elastic structure alterations in atherosclerotic arteries in minipigs: plaque proximity and arterial site specificity. Matrix Biol 1997;15(7):455–67.

Barth A. The infrared absorption of amino acid side chains. Prog Biophys Mol Biol 2000;74(3–5):141–73.

Barth A. Infrared spectroscopy of proteins. Biochim Biophys Acta 2007;1767(9):1073–101.

Blaise S, Romier B, Kawecki C, Ghirardi M, Rabenoelina F, Baud S, et al. Elastin-derived peptides are new regulators of insulin resistance development in mice. Diabetes 2013;62(11):3807–16.

Bonnier F, Rubin S, Ventéo L, Krishna CM, Pluot M, Baehrel B, et al. In-vitro analysis of normal and aneurismal human ascending aortic tissues using FT-IR microspectroscopy. Biochim Biophys Acta 2006;1758(7):968–73.

Bonnier F, Rubin S, Debelle L, Ventéo L, Pluot M, Baehrel B, et al. FTIR protein secondary structure analysis of human ascending aortic tissues. J Biophoton 2008;1(3):204–14.

Bromme D. Production and activation of recombinant papain-like cysteine proteases. Methods 2004;32(2):199–206.

Burns-Kurtis CL, Olzinski AR, Needle S, Fox JH, Capper EA, Kelly FM, et al. Cathepsin S expression is up-regulated following balloon angioplasty in the hypercholesterolemic rabbit. Cardiovasc Res 2004;62(3):610–20.

Caglic D, Pungercar JR, Pejler G, Turk V, Turk B. Glycosaminoglycans facilitate procathepsin B activation through disruption of propeptide-mature enzyme interactions. J Biol Chem 2007;282(45):33076–85.

Cal R, Castellano J, Revuelta-López E, Aledo R, Barriga M, Farré J, et al. Low-density lipoprotein receptor-related protein 1 mediates hypoxia-induced very low density lipoprotein-cholesteryl ester uptake and accumulation in cardiomyocytes. Cardiovasc Res 2012;94(3):469–79.

Cheng XW, Obata K, Kuzuya M, Izawa H, Nakamura K, Asai E, et al. Elastolytic cathepsin induction/activation system exists in myocardium and is upregulated in hypertensive heart failure. Hypertension 2006;48(5):979–87.

Claycomb WC, Lanson NA, Stallworth BS, Egeland DB, Delcarpio JB, Bahinski A, et al. HL-1 cells: a cardiac muscle cell line that contracts and retains phenotypic characteristics of the adult cardiomyocyte. Proc Natl Acad Sci USA 1998;95(6):2979–84.

Davis EC, Mecham RP. Intracellular trafficking of tropoelastin. Matrix Biol 1998;17(4):245–54.

Debelle L, Alix AJ, Jacob MP, Huvenne JP, Berjot M, Sombret B, et al. Bovine elastin and kappa-elastin secondary structure determination by optical spectroscopies. J Biol Chem 1995;270(44):26099–103.

Debelle L, Tamburro AM. Elastin: molecular description and function. Int J Biochem Cell Biol 1999;31(2):261–72.

Dhalla NS, Saini-Chohan HK, Rodriguez-Leyva D, Elimban V, Dent MR, Tappia PS. Subcellular remodelling may induce cardiac dysfunction in congestive heart failure. Cardiovasc Res 2009;81(3):429–38.

Díez J. Altered degradation of extracellular matrix in myocardial remodelling: the growing role of cathepsins and cystatins. Cardiovasc Res 2010;87(4):591–2.

Driessen C, Bryant RA, Lennon-Duménil AM, Villadangos JA, Bryant PW, Shi GP, et al. Cathepsin S controls the trafficking and maturation of MHC class II molecules in dendritic cells. J Cell Biol 1999;147(4):775–90.

Eghbali M. Cardiac fibroblasts: function, regulation of gene expression, and phenotypic modulation. Basic Res Cardiol 1992;87(Suppl 2):183–9.

Ferry JD. Viscoelastic properties of polymers. 3rd ed Wiley; 1980.

Floquet N, Héry-Huynh S, Dauchez M, Derreumaux P, Tamburro AM, Alix AJP. Structural characterization of VGVAPG, an elastin-derived peptide. Biopolymers 2004;76(3):266–80.

Fomovsky GM, Thomopoulos S, Holmes JW. Contribution of extracellular matrix to the mechanical properties of the heart. J Mol Cell Cardiol 2010;48(3):490–6.

Foster JA, Rubin L, Kagan HM, Franzblau C, Bruenger E, Sandberg LB. Isolation and characterization of cross-linked peptides from elastin. J Biol Chem 1974;249(19):6191–6.

Fulop T, Khalil A, Larbi A. The role of elastin peptides in modulating the immune response in aging and age-related diseases. Pathol Biol 2012;60(1):28–33.

Gayral S, Garnotel R, Castaing-Berthou A, Blaise S, Fougerat A, Berge E, et al. Elastin-derived peptides potentiate atherosclerosis through the immune Neu1-PI3Kγ pathway. Cardiovasc Res 2014;102(1):118–27.

Ge J, Zhao G, Chen R, Li S, Wang S, Zhang X, et al. Enhanced myocardial cathepsin B expression in patients with dilated cardiomyopathy. Eur J Heart Fail 2006;8(3):284–9.

Goldberg IJ. Clinical review 124: diabetic dyslipidemia: causes and consequences. J Clin Endocrinol Metab 2001;86(3):965–71.

Goldberg IJ, Eckel RH, McPherson R. Triglycerides and heart disease: still a hypothesis? Arterioscler Thromb Vasc Biol 2011;31(8):1716–25.

Granér M, Siren R, Nyman K, Lundbom J, Hakkarainen A, Pentikäinen MO, et al. Cardiac steatosis associates with visceral obesity in nondiabetic obese men. J Clin Endocrinol Metab 2013;98(3):1189–97.

Gupta V, Grande-Allen KJ. Effects of static and cyclic loading in regulating extracellular matrix synthesis by cardiovascular cells. Cardiovasc Res 2006;72(3):375–83.

Hale JE, Schroeder F. Differential scanning calorimetry and fluorescence probe investigations of very low density lipoprotein from the isolated perfused rat liver. J Lipid Res 1981;22(5):838–51.

Hayden MR, Chowdhury N, Govindarajan G, Karuparthi PR, Habibi J, Sowers JR. Myocardial myocyte remodeling and fibrosis in the cardiometabolic syndrome. J Cardiometab Syndr 2006;1(5):326–33.

Henderson BC, Sen U, Reynolds C, Moshal KS, Ovechkin A, Tyagi N, et al. Reversal of systemic hypertension-associated cardiac remodeling in chronic pressure overload myocardium by ciglitazone. Int J Biol Sci 2007;3(6):385–92.

Herberhold H, Winter R. Temperature- and pressure-induced unfolding and refolding of ubiquitin: a static and kinetic Fourier transform infrared spectroscopy study. Biochemistry 2002;41(7):2396–401.

Hoeve CA, Flory PJ. The elastic properties of elastin. Biopolymers 1974;13(4):677–86.

Hu X, Kaplan D, Cebe P. Determining beta-sheet crystallinity in fibrous proteins by thermal analysis and infrared spectroscopy. Macromolecules 2006;39(18):6161–70.

Hu X, Wang X, Rnjak J, Weiss AS, Kaplan DL. Biomaterials derived from silk-tropoelastin protein systems. Biomaterials 2010;31(32):8121–31.

Jarauta E, Mateo-Gallego R, Gilabert R, Plana N, Junyent M, de Groot E, et al. Carotid atherosclerosis and lipoprotein particle subclasses in familial hypercholesterolaemia and familial combined hyperlipidaemia. Nutr Metab Cardiovasc Dis 2012;22(7):591–7.

Kadowaki H, Patton GM, Robins SJ. Metabolism of high density lipoprotein lipids by the rat liver: evidence for participation of hepatic lipase in the uptake of cholesteryl ester. J Lipid Res 1992;33(11):1689–98.

Kozel BA, Rongish BJ, Czirok A, Zach J, Little CD, Davis EC, et al. Elastic fiber formation: a dynamic view of extracellular matrix assembly using timer reporters. J Cell Physiol 2006;207(1):87–96.

Krilov D, Balarin M, Kosović M, Gamulin O, Brnjas-Kraljević J. FT-IR spectroscopy of lipoproteins—a comparative study. Spectrochim Acta A Mol Biomol Spectrosc 2009;73(4):701–6.

Li B, Daggett V. Molecular basis for the extensibility of elastin. J Muscle Res Cell Motil 2002;23(5-6):561–73.

Li B, Alonso DOV, Daggett V. Stabilization of globular proteins via introduction of temperature-activated elastin-based switches. Structure 2002;10(7):989–98.

Lillie MA, Gosline JM. Effects of lipids on elastin's viscoelastic properties. Biopolymers 2002a;64(3):127–38.

Lillie MA, Gosline JM. The viscoelastic basis for the tensile strength of elastin. Int J Biol Macromol 2002b;30(2):119–27.

Llorente-Cortés V, Otero-Viñas M, Badimon L. Differential role of heparan sulfate proteoglycans on aggregated LDL uptake in human vascular smooth muscle cells and mouse embryonic fibroblasts. Arterioscler Thromb Vasc Biol 2002;22(11):1905–11.

Llorente-Cortés V, Otero-Viñas M, Camino-López S, Costales P, Badimon L. Cholesteryl esters of aggregated LDL are internalized by selective uptake in human vascular smooth muscle cells. Arterioscler Thromb Vasc Biol 2006;26(1):117–23.

Llorente-Cortés V, Otero-Viñas M, Camino-López S, Llampayas O, Badimon L. Aggregated low-density lipoprotein uptake induces membrane tissue factor procoagulant activity and microparticle release in human vascular smooth muscle cells. Circulation 2004;110(4):452–9.

Mecham RP. Introduction: catalyzing matrix stability. Am J Respir Cell Mol Biol 1991;5(3):205.

Nara M, Okazaki M, Kagi H. Infrared study of human serum very-low-density and low-density lipoproteins. Implication of esterified lipid C=O stretching bands for characterizing lipoproteins. Chem Phys Lipids 2002;117(1–2):1–6.

Nielsen MS, Brejning J, García R, Zhang H, Hayden MR, Vilaró S, et al. Segments in the C-terminal folding domain of lipoprotein lipase important for binding to the low density lipoprotein receptor-related protein and to heparan sulfate proteoglycans. J Biol Chem 1997;272(9):5821–7.

O'Rourke M. Arterial aging: pathophysiological principles. Vasc Med 2007;12(7):329–41.

Obermajer N, Jevnikar Z, Doljak B, Kos J. Role of cysteine cathepsins in matrix degradation and cell signalling. Connect Tissue Res 2008;49(3):193–6.

Ontong P, Hatada Y, Taniguchi S, Kakizaki I, Itano N. Effect of a cholesterol-rich lipid environment on the enzymatic activity of reconstituted hyaluronan synthase. Biochem Biophys Res Commun 2014;443(2):666–71.

Panagopoulou A, Kyritsis A, Vodina M, Pissis P. Dynamics of uncrystallized water and protein in hydrated elastin studied by thermal and dielectric techniques. Biochem Biophys Acta 2013;1834(6):977–88.

Pillutla P, Hwang YC, Augustus A, Yokoyama M, Yagyu H, Johnston TP, et al. Perfusion of hearts with triglyceride-rich particles reproduces the metabolic abnormalities in lipotoxic cardiomyopathy. Am J Physiol Endocrinol Metab 2005;288(6):E1229–35.

Pluot M, Baehrel B, Manfait M, Rubin S, Bonnier F, Sandt C, et al. Analysis of structural changes in normal and aneurismal human aortic tissues using FTIR microscopy. Biopolymers 2007;89(2):160–9.

Podet EJ, Shaffer DR, Gianturco SH, Bradley WA, Yang CY, Guyton JR. Interaction of low density lipoproteins with human aortic elastin. Arterioscler Thromb 1991;11(1):116–22.

Popescu M-C, Vasile C, Craciunescu O. Structural analysis of some soluble elastins by means of FT-IR and 2D IR correlation spectroscopy. Biopolymers 2010;93(12):1072–84.

Prassl R, Schuster B, Abuja PM, Zechner M, Kostner GM, Laggner P. A comparison of structure and thermal behavior in human plasma lipoprotein(a) and low-density lipoprotein. Calorimetry and small-angle X-ray scattering. Biochemistry 1995;34(11):3795–801.

Puett D, Ciferri A, Bianchi E, Hermans J. Helix formation of poly-L-lysine thiocyanate in aqueous solutions. J Phys Chem 1967;71(12):4126–8.

Pungercar JR, Caglic D, Sajid M, Dolinar M, Vasiljeva O, Pozgan U, et al. Autocatalytic processing of procathepsin B is triggered by proenzyme activity. FEBS J 2009;276(3):660–8.

Rijzewijk LJ, van der Meer RW, Smit JWA, Diamant M, Bax JJ, Hammer S, et al. Myocardial steatosis is an independent predictor of diastolic dysfunction in type 2 diabetes mellitus. J Am Coll Cardiol 2008;52(22):1793–9.

Samouillan V, Dandurand J, Lamure A, Maurel E, Lacabanne C, Gerosa G, et al. Thermal analysis characterization of aortic tissues for cardiac valve bioprostheses. J Biomed Mater Res 1999;46(4):531–8.

Samouillan V, Dandurand J, Nasarre L, Badimon L, Lacabanne C, Llorente-Cortés V. Lipid loading of human vascular smooth muscle cells induces changes in tropoelastin protein levels and physical structure. Biophys J 2012;103(3):532–40.

Sandberg LB. Elastin structure in health and disease. Int Rev Connect Tissue Res 1976;7:159–210.

Sartipy P, Camejo G, Svensson L, Hurt-Camejo E. Phospholipase A(2) modification of low density lipoproteins forms small high density particles with increased affinity for proteoglycans and glycosaminoglycans. J Biol Chem 1999;274(36):25913–20.

Sato S, Ashraf M, Millard RW, Fujiwara H, Schwartz A. Connective tissue changes in early ischemia of porcine myocardium: an ultrastructural study. J Mol Cell Cardiol 1983;15(4):261–75.

Seo T, Al-Haideri M, Treskova E, Worgall TS, Kako Y, Goldberg IJ, et al. Lipoprotein lipase-mediated selective uptake from low density lipoprotein requires cell surface proteoglycans and is independent of scavenger receptorclass B type 1. J Biol Chem 2000;275(39):30355–62.

Servaty R, Schiller J, Binder H, Arnold K. Hydration of polymeric components of cartilage—an infrared spectroscopic study on hyaluronic acid and chondroitin sulfate. Int J Biol Macromol 2001;28(2):121–7.

Sionkowska A, Skopinska-Wisniewska J, Gawron M, Kozlowska J, Planecka A. Chemical and thermal cross-linking of collagen and elastin hydrolysates. Int J Biol Macromol 2010;47(4):570–7.

Staniszewska E, Malek K, Baranska M. Rapid approach to analyze biochemical variation in rat organs by ATR FTIR spectroscopy. Spectrochim Acta A Mol Biomol Spectrosc 2014;118:981–6.

Sun M, Chen M, Liu Y, Fukuoka M, Zhou K, Li G, et al. Cathepsin-L contributes to cardiac repair and remodelling post-infarction. Cardiovasc Res 2011;89(2):374–83.

Swarnakar S, Beers J, Strickland DK, Azhar S, Williams DL. The apolipoprotein E-dependent low density lipoprotein cholesteryl ester selective uptake pathway in murine adrenocortical cells involves chondroitin sulfate proteoglycans and an alpha 2-macroglobulin receptor. J Biol Chem 2001;276(24):21121–8.

Tamburro AM, Pepe A, Bochicchio B. Localizing alpha-helices in human tropoelastin: assembly of the elastin puzzle. Biochemistry 2006;45(31):9518–30.

Van der Donckt C, Van Herck JL, Schrijvers DM, Vanhoutte G, Verhoye M, Blockx I, et al. Elastin fragmentation in atherosclerotic mice leads to intraplaque neovascularization, plaque rupture, myocardial infarction, stroke, and sudden death. Eur Heart J 2014., http://dx.doi.org/10.1093/eurheartj/ehu041 [in press].

Vassiliou G, McPherson R. A novel efflux-recapture process underlies the mechanism of high-density lipoprotein cholesteryl ester-selective uptake mediated by the low-density lipoprotein receptor-related protein. Arterioscler Thromb Vasc Biol 2004;24(9):1669–75.

Yu VS, Kalnin NN. Quantitative IR spectrophotometry of peptide compounds in water (H_2O) solutions. I. Spectral parameters of amino acid residue absorption bands. Biopolymers 1990;30(13–14):1243–57.

Vilalta M, Jorgensen C, Dégano IR, Chernajovsky Y, Gould D, Noël D, et al. Dual luciferase labelling for non-invasive bioluminescence imaging of mesenchymal stromal cell chondrogenic differentiation in demineralized bone matrix scaffolds. Biomaterials 2009;30(28):4986–95.